Properties of niobium–titanium superconducting wires with Nb artificial pinning centers

R. W. Heussner,[a] C. Bormio Nunes,[b] P. J. Lee, and D. C. Larbalestier[a]
Applied Superconductivity Center, University of Wisconsin-Madison, 1500 Engineering Drive, Madison, Wisconsin 53706

P. D. Jablonski
Teledyne Wah Chang, Albany, Oregon 97321

(Received 5 March 1996; accepted for publication 3 May 1996)

Artificial pinning center (APC) Nb 47 wt % Ti composite wires containing 24 vol % Nb pins were characterized as the wire diameter was reduced. As the nominal pin diameter d_p was reduced from 165 to 15 nm, the nominally round pins transformed into ribbons with a relatively wide distribution in thickness, as compared to the α-Ti ribbons in optimized, conventionally processed Nb 47 wt % Ti. The maximum in the bulk flux pinning force F_p of 25 GN/m^3 (4.2 K, 2.5 T) occurred at $d_p=40$ nm, for which the measured Nb ribbon thickness ranged from 1 to 16 nm. This F_p value was about one third higher than that found in the best conventional Nb 47 wt % Ti. The upper critical magnetic field H_{c2}, measured by magnetization, decreased from 10.3 to 9 T as the Nb pins became proximity-effect coupled to the matrix. To better compare APC and conventional wires, we measured the properties of the best APC wire at a reduced temperature so that its H_{c2} was the same as H_{c2}(4.2 K) for Nb 47 wt % Ti. The peak value of F_p was then 36 GN/m^3 at 3 T, almost twice the maximum value yet reported for conventional Nb–Ti (~19 GN/m^3 at 5 T). In spite of the pinning force curve remaining sharply peaked at lower fields, the equalized 5 T critical current density was 4600 A/mm^2, some 25% higher than the best values of conventional Nb–Ti. These properties demonstrate the strong potential of APC composites. © *1996 American Institute of Physics.* [S0021-8979(96)09615-6]

I. INTRODUCTION

The critical current density J_c in conventionally processed Nb 47 wt % Ti wires appears to be at its limit since no significant improvements in J_c have been made in recent years. The thermomechanical processing steps for optimizing J_c have been extensively examined. A first step towards optimizing the flux pinning in Nb–Ti is to develop ~20–25 vol % of 100–200 nm diameter, normal α-Ti precipitates in the parent β-Nb–Ti matrix through several heat treatment and drawing steps.[1,2] The final step is to reduce the ellipsoid-shaped precipitates into long ribbons by wire drawing. Optimum flux pinning occurs with 1–2 nm thick ribbons separated by ~5 nm.[3,4] J_c increases linearly with the volume fraction of α-Ti precipitate up to 25 vol %,[5] an amount which represents the thermodynamic and/or practical kinetic limit in Nb 47 wt % Ti.

One route to higher performance is to replace the naturally produced α-Ti pins with better, so-called artificial pinning center (APC) superconductor designs which do not suffer from thermodynamic or kinetic restrictions and thus offer greater flexibility in the choice of pinning center composition, volume fraction, and distribution. A variety of methods[6–13] have been used to incorporate artificial pinning centers into Nb–Ti and some considerable successes have been achieved. A multilayered APC structure consisting of Nb 50 wt % Ti with 28 vol % Nb[9] achieved 4250 A/mm^2 (5 T, 4.2 K), the highest value ever reported for a round Nb–Ti wire. This high value was achieved despite the fact that the composite upper critical magnetic field H_{c2} was ~1 T less than that of Nb 47 wt % Ti.

However, present APC designs have some drawbacks, not the least of which results from the operation of the proximity effect.[14,15] Most existing APC designs use Nb 47–50 wt % Ti with 20–30 vol % of pins, generally Nb pins. At optimum J_c sizes, the pins are sufficiently small for proximity-effect coupling to occur. Proximity-effect coupling of the pins to the matrix homogenizes the H_{c2} and the critical temperature T_c, changing them from values of the matrix composition to values representing a composite average.[3] In the case of Nb pins coupled to Nb 47 wt % Ti, Nb-rich composite mixtures have a slightly higher T_c but a considerably reduced H_{c2}.[7,9,12,16,17] Other pin materials, such as Cu,[7] can reduce both values in even more marked fashion. However, recent multilayers of Nb 47 wt % Ti with Cu pins exhibited no H_{c2} depression for the highest J_c sample and achieved a maximum F_p(4.2 K, H) of 46 GN/m^3 for 30 nm thick Nb–Ti and 10 nm thick Cu layers.[18] Proximity-effect coupling also occurs in conventional Nb–Ti, but in this case the overall composition is close to that of maximum H_{c2} and the proximity effect exerts a beneficial effect, serving to restore the high H_{c2} that was lost during the composition changes that accompany the precipitation heat treatments. The key to optimizing H_{c2} thus appears to be in avoiding an overall composition which departs significantly from the Nb 44–48 wt % Ti range at which H_{c2} reaches its peak.

Another important difference between APC and conventional wires lies in the shape of the bulk flux pinning curves, particularly the value of field $H_{\max}$ at which the maximum pinning force $F_{p\max}$ occurs. Conventional composites peak at ~$0.5H_{c2}$ while APC composites most often peak at

[a]Materials Science Program.
[b]On leave from FAENQUIL/DEMAR, 12600-000 Lorena-SP, Brazil.

 0021-8979/96/80(3)/1640/7/$10.00

$\sim 0.25 H_{c2}$. Flux pinning in conventional Nb–Ti has long been explained with fluxon core interaction models,[3,4,6,7] from which a peak in $F_{p\max}$ at $H_{\max} \sim 0.5 H_{c2}$ appears naturally. Since APC pinning arrays are in principal, very similar to conventional arrays, this difference raised many questions. In particular, it has raised the question as to whether the dominant pinning mechanism is not a magnetic one, rather than a fluxon core one.[19–21] The importance of magnetic pinning interactions has recently been completely reevaluated and a new model[20] has been introduced to describe the behavior of both conventional and APC Nb–Ti. Cooley *et al.*[20] explain the difference in bulk pinning force curves between conventional and APC Nb–Ti as resulting from the proximity length of pure Nb pins being much longer than that of α-Ti pins. This new model makes testable predictions of optimum pin design for any Nb–Ti composite, directly proposing that APC designs of Nb–Ti can be further optimized by reducing the electron mean free path of the pin.

This paper describes the development of the microstructure and superconducting properties for an APC composite wire having a Nb 47 wt % Ti with 24 vol % of Nb pinning centers. The goal has been to make a thorough nanoscale microstructural characterization so that the pinning center size and shape at optimum wire sizes is known and not just assumed. Such characterizations are seldom performed at optimum size. A second aspect of the study was to measure the J_c, F_p, and H_{c2} at reduced temperatures, not just at 4.2 K, so that the properties of conventional and APC wires could be compared at constant H_{c2}. To perform the reduced temperature study we relied primarily on magnetization measurements. During measurement we found a very strong sensitivity of the magnitude and shape of the hysteretic magnetization on sample length. An experimental and theoretical analysis of this effect, showing the role that the anisotropic pinning nanostructure has on the longitudinal and transverse critical current densities of optimized Nb–Ti wires, is presented in Ref. 22.

II. EXPERIMENT

An APC composite containing a matrix of Nb 47 wt % Ti and 24 vol % of round Nb pins was fabricated using the rod bundling process discussed previously.[12] Thirty-one 1 mm diam Nb rods were arranged in a hexagonal array within a bundle of 96 Nb 47 wt % Ti rods. This 127 rod stack was canned in Cu and hydrostatically extruded at 650 °C using an area reduction ratio of 15. The extruded wire was drawn to 1 mm diam, cut lengthwise into 127 pieces, and the Cu was dissolved away in a 1:1 mixture of HNO_3 and H_2O. The hexagonal shaped Nb–Ti/Nb filaments were restacked, canned in Cu, and a second extrusion was made under the same conditions. After a further draw, restack and a third extrusion sequence, the monofilament wire contained 5×10^5 Nb pinning centers. A part of this wire was drawn to 0.08 mm diam, while the rest was cut into seven pieces and extruded for a fourth time. The fourth extrusion wire was also drawn to 0.08 mm diam.

Critical currents I_c were measured with a standard four point probe using a voltage tap spacing of 22 or 33 cm and a resistivity criterion of 10^{-14} Ω m. Transport critical current densities J_{ct} were determined by dividing the critical currents by the measured superconductor cross-sectional area. Copper to superconductor area ratios were determined by weighing a length of wire sample, etching away the Cu matrix, and reweighing. The calculated *nominal* pinning center diameter d_p is commonly used to describe the pinning center dimension, it is given by

$$d_p = \frac{d_w}{\sqrt{N(1+R)}}, \tag{1}$$

where d_w is the wire diameter, N is the number of rods (e.g., $127\times127\times127$ for the third extrusion composite) and R is the Cu to superconductor ratio. However, as the microscopy in Figs. 1(a)–1(e) shows, the actual pinning center thickness was substantially less than the round wire approximation d_p for all optimized wires.

Magnetic moments were measured on wire samples using a vibrating sample magnetometer (VSM). Long wire samples, ranging from 56 mm in length for the 0.360 mm diam wire to 300 mm for the 0.080 mm diam wires, were wound into 3 mm diam, 1 mm long open circuit coils. Long wire samples were used for two reasons. Longer samples provide a larger sample moment, giving higher signal resolution. More importantly, it has been demonstrated for this same set of samples,[22] that the magnetization of APC wires can be a very strong function of the wire length-to-diameter ratio. As the measured length is increased, so is the agreement between the J_{ct} and the magnetization critical current density $J_{\rm cm}$ improved. The sample-length dependence comes from the fact that the magnetization-induced current must cross the filament in a direction perpendicular to the wire axis towards the ends of each filament and because the anisotropic pinning nanostructure of the wires produces a J_c perpendicular to the axis of the pinning centers which is up to $\sim$100 times less than that flowing parallel to the pinning centers along the wire axis. To obviate these concerns, moment measurements were made with the applied field parallel to the coil axis on long samples,[22] so that the field was perpendicular to the long wire axis and currents were induced to flow along the whole wire length. A field sweep rate of 0.05 T/s was used, except near H_{c2}, where it was reduced to 0.02 T/s to increase resolution in the region of magnetization loop closure. The magnitude of the hysteretic moment depended only weakly on the field sweep rate for these APC monofilament samples. Magnetization M was calculated by dividing the moment by the superconductor volume. Magnetization critical current densities were derived from the magnetization loops of the long samples using the Bean model for a cylindrical superconductor in perpendicular field[23]

$$J_{\rm cm}(H,T) = \frac{3\pi\Delta M(H,T)}{4d_f}, \tag{2}$$

where ΔM is the width of the magnetization hysteresis and d_f is the filament diameter. Magnetization runs were made at temperatures from 3 to 10 K in fields up to 12 T. Transverse wire cross sections were analyzed by scanning (SEM), field emission scanning (FESEM), and transmission electron microscopy (TEM).

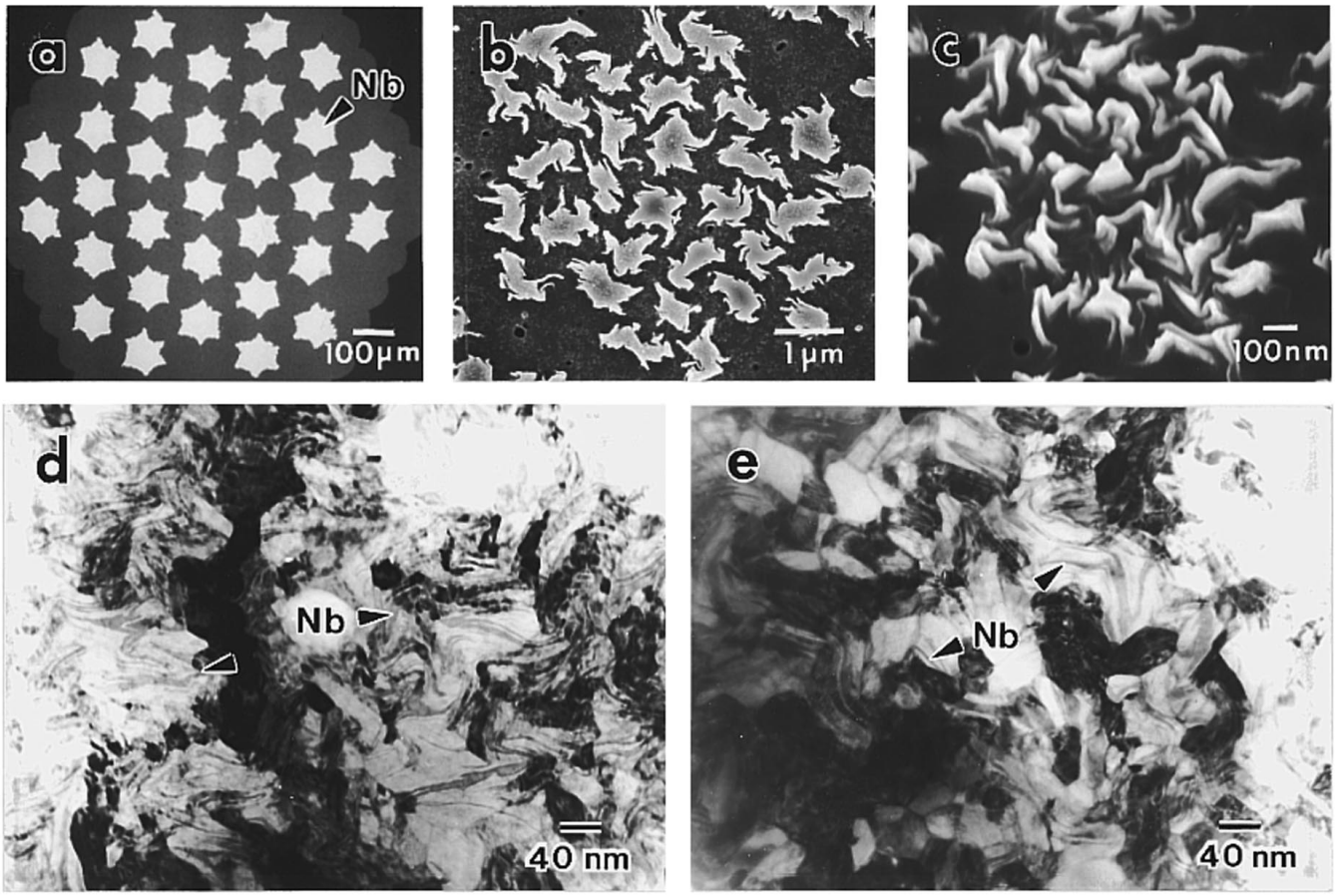

FIG. 1. SEM images of the Nb pinning center array at (a) $d_p=100$ μm, (b) 600 nm and (c) 100 nm and TEM images at $d_p=40$ nm for the third (d) and fourth (e) extrusion composites. The micrographs show the development of the round pinning centers into highly aspected ribbons. At $d_p=40$ nm the actual measured pin thickness ranged from 1 to 16 nm for both the third and fourth extrusion composites.

III. RESULTS

Figure 1 shows the microstructural development of the Nb pinning centers as a function of the nominal pin diameter. Following the first extrusion, at $d_p=100$ μm [Fig. 1(a)], the pins had a hexagonal shape with an irregular surface. The sixfold star shape comes from the deformation of the round wire stack during extrusion. After the fourth extrusion, at $d_p=600$ nm [Fig. 1(b)], the pin shape had changed and fine tendrils extended from the pin surfaces. The hexagonal pin array, though degraded, was still visible. At $d_p=100$ nm [Fig. 1(c)], the pins had deformed into ribbons with aspect ratios of 3:1–10:1. Figures 1(d) and 1(e) show TEM images of the pins at $d_p=40$ nm for the third and fourth extrusion composites, respectively. The microstructural contrast in the TEM images comes principally from two sources. One is Bragg diffraction from suitably oriented Nb–Ti grains, these being the approximately equiaxed features seen prominently in Fig. 1(e). The residual contrast is dominated by the local atomic number. Nb ribbons are thus darker than the Nb–Ti matrix and are visible within the Nb–Ti grains. The Nb ribbons of both wires exhibit large aspect ratios and a measured pin thickness which varies from <1 to 16 nm. In neither of these pictures is the original hexagonal arrangement of the pins visible. At $d_p=15$ nm, some 1 nm thick pins could be observed in TEM images, but the pins were very difficult to discern at this stage.

Figure 2 shows the transport critical current density versus d_p for applied fields ranging from 1 to 7 T. Two sets of data are shown: that for the third extrusion covers the range of d_p from 165 to 40 nm and that for the fourth ranges from 60 to 15 nm. J_c increases almost continuously (except at 1 T) with decreasing d_p for the third extrusion composite. At 1 T, the peak J_c was 20 kA/mm^2 for $d_p=50$ nm, while at 5 T, it was 3200 A/mm^2 for $d_p=35$ nm. In the pin diameter interval where the third and fourth extrusion data sets overlap, that is $d_p=40$–60 nm, there is poor agreement. Furthermore, the disagreement is compounded by the presence of a crossover in behavior as the field is increased. From 1 to 3 T the third extrusion composite J_c values exceed those of the fourth. From 3 to 5 T, crossover points are indicated by the vertical arrows in Fig. 2 and from 5 to 7 T, the fourth extrusion J_c values exceed those of the third. The fourth extrusion composite exhibits J_c peaks at successively smaller d_p values as the field is increased; peaks of 40, 35, 25, and 17 nm occur for fields of 4, 5, 6, and 7 T, respectively. As is clear from Fig. 1, the actual pin thickness is, in all cases, much smaller than d_p.

Figure 3 shows the bulk flux pinning force $F_p(H, 4.2\ \mathrm{K})=J_c(H)\times\mu_0 H$ of the APC composite as d_p is reduced from 165 to 15 nm. The large arrows follow the maximum in F_p as the pin size is reduced. For $d_p=165$ nm, the largest pin diameter wire measured, $F_p(H)$ decreased almost linearly

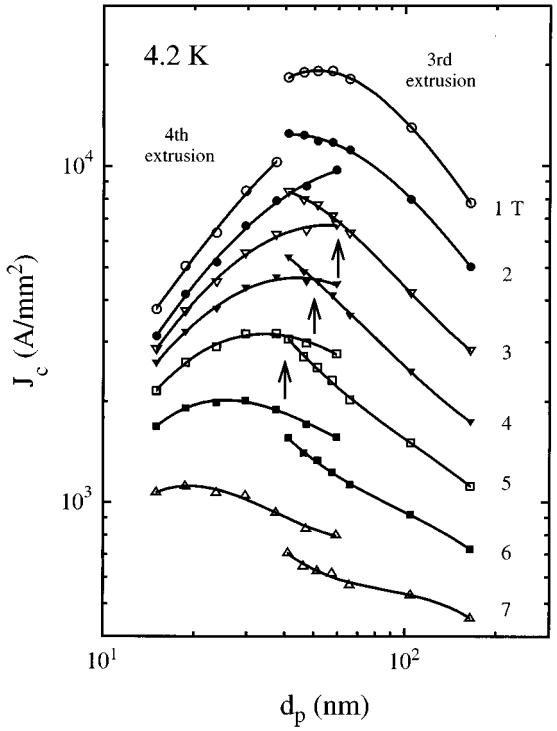

FIG. 2. J_c vs d_p for applied fields from 1 to 7 T. The curve sets from 165 to 40 and 60 to 15 nm correspond to the third and fourth extrusion composites, respectively. The vertical arrows indicate overlap points between the two curve sets.

with increasing field. As the pin size was reduced, a low field maximum in $F_p(H)$ emerged. The maximum value F_p of 25 GN/m^3 occurred at 2.5 T for $d_p=40$ nm. As the pin size was reduced further, the peak in $F_p(H)$ shifted to higher fields and the shape of $F_p(H)$ tended towards that of conventionally processed Nb 47 wt % Ti, but the peak magnitude declined rapidly, as seen for $d_p=15$ nm.

Figure 4 shows the magnetization $M(H, 4.2\ \mathrm{K})$ near H_{c2}

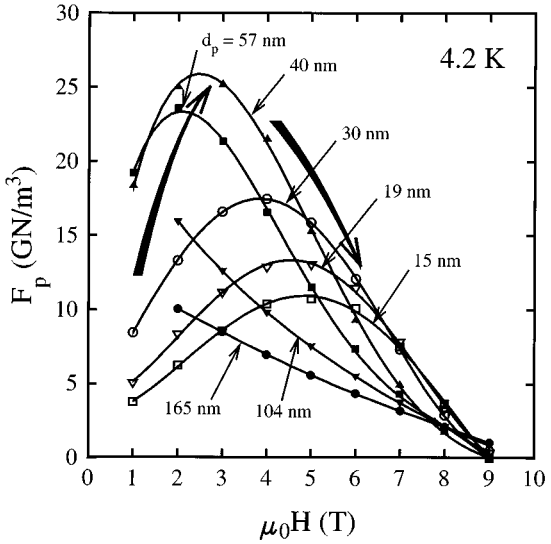

FIG. 3. F_p vs $\mu_0 H$ as a function of d_p as derived from the transport critical current measurements. The filled and open symbols correspond to third and fourth extrusion composites, respectively. The long arrows follow the maximum in F_p as the pin size d_p is reduced.

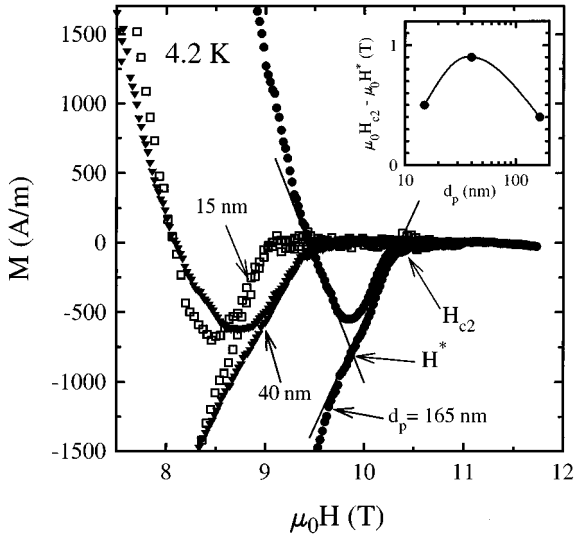

FIG. 4. M vs $\mu_0 H$ near H_{c2} for $d_p=165$, 40, and 15 nm. The irreversibility field H^* is defined as the field at which the linear extrapolation of the positive magnetization arm intersects the negative arm. H_{c2} is defined as the field at which the negative arm intersects $M=0$. A residual paramagnetic moment was subtracted from each magnetization curve. The inset graph shows how the quantity $H_{c2}-H^*$ changes as the nominal pin diameter is reduced.

for $d_p=165$, 40, and 15 nm. In addition to the hysteretic magnetization caused by flux pinning, there was a small ($\chi\sim 2\times 10^{-4}$) orbital paramagnetic moment contribution from the Nb–Ti. This contribution, together with a small signal from the Pyrex sample rod, were identified by making measurements at 10 K, above the critical temperature T_c of 9.2 K for Nb 47 wt % Ti. Both contributions were subtracted from the data of Fig. 4. These data show that the hysteresis loop does not close at H_{c2} but at a lower field, H^*. This irreversibility field H^* was experimentally defined as the field at which the linear extrapolation of the positive magnetization arm intersects the negative arm, thus following similar conventions used by Suenaga *et al.*[24] for conventional Nb–Ti and Bonney *et al.*[25] for $SnMo_6S_8$. H_{c2} is defined as the field at which a linear extrapolation of the negative arm intersects $M=0$. Both constructions are illustrated in Fig. 4.

Table I lists the measured H^* and H_{c2} values as a function of nominal pin diameter and temperature. The inset graph of Fig. 4 shows how the quantity $H_{c2}-H^*$ changes as the nominal pin diameter is reduced. For the 165 and 15 nm diam pins, the difference between H^* and H_{c2} is ~0.5 T. At $d_p=40$ nm, the optimum pin size, the difference is ~0.9 T. For an optimized, conventionally processed wire at 4.2 K,[26] H^* and H_{c2} were measured to be 10.2 and 10.7 T, respectively, values which are 1.6 and 1.2 T higher than those measured for the highest flux pinning ($d_p=40$ nm) APC sample. This strong suppression of both H^* and H_{c2} in the APC composite complicates comparison of APC and conventional wire properties.

IV. DISCUSSION

A. Microstructure

In this study, as in the few other studies which have explicitly observed the microstructure at optimum wire

TABLE I. Magnetization H^* and H_{c2} values as a function of d_p and temperature for the APC wires at $d_p=165$, 40, and 15 nm and for an optimized, conventionally processed Nb 47 wt % Ti wire at 4.2 K.

T(K)→	4.2 K			3.5 K		3.0 K	
d_p (nm)	H_{c2} (T)	H^* (T)	$H_{c2}-H^*$	H_{c2}	H^*	H_{c2}	H^*
165	10.3	9.9	0.4	⋯	⋯	⋯	⋯
40	9.5	8.6	0.9	10.7	9.6	⋯	10.3
15	9.0	8.5	0.5	9.8	9.2	11.0	10.3
Conventional	10.7	10.2	0.5	⋯	⋯	⋯	⋯

sizes,[1,3,10,11] it is abundantly clear that the real pin thickness is considerably smaller than the round wire approximation, d_p. The ribbonlike shape developed by the Nb pinning centers is a general consequence of the ⟨110⟩ drawing texture which develops in body centered cubic (bcc) metals subjected to the axially symmetric deformation of wire drawing.[27–29] In the early stages of drawing, individual grains rotate, such that a ⟨110⟩ direction is aligned with the drawing axis. Slip is then restricted to the two ⟨111⟩ directions which lie within the {110} plane containing the ⟨110⟩ texture. The resultant plane strain deformation, combined with the requirement of grain boundary continuity, forces the grains to intercurl, slowly transforming into ribbons. In the case of the conventionally produced $\alpha+\beta$ two-phase microstructure, the bcc β-Nb–Ti grain texture development causes the hexagonal close packed α-Ti precipitates to transform into ribbons. In the APC composite, both Nb and Nb–Ti are bcc, so it is likely that both pin and matrix contribute to the ribboning.

It is worth noting that the pin shape seen here, at least in the latter stages of development, parallels that seen in an earlier study by Cooley *et al.*[10,16] of a somewhat similar APC composite. In that case, the pins of Nb 1 wt % Ti were inserted into gun-barrel-drilled holes and, aside from the initial warm extrusion of the original 150 mm diam Nb 47 wt % Ti/Nb 1 wt % Ti, all subsequent composite fabrication was done by cold drawing. The shape of nominal 600 and 100 nm diam pins of the present composite are comparable to the shape of the 200 and 32 nm diam pins of the earlier study. The difference in the onset of pin shape degradation is likely due to differences in processing methods, for in the present case, the pins were given an anneal at ~1 mm diameter just prior to the stacking of the billet and three or four warm (650 °C) extrusion steps were then used during wire reduction, thereby increasing the tendency for polygonization or recovery of the Nb–Ti grains, either of which would increase the ratio of the Nb–Ti grain size to Nb pin diameter and cause more rapid pin shape degradation. Thus, the use of the nominal pin diameter as a quantitative tool can be somewhat misleading, since two APC composites of not greatly dissimilar design can have significantly different pinning microstructures for the same value of d_p. However, the use of d_p is so widespread in the literature and there is so little quantitative microscopy near optimum sizes that it is still useful to report properties as a function of d_p. Quantitative understanding of the dependence of properties on microstructure clearly requires observation of the microstructure.

The maximum F_p for the APC composite occurs at $d_p=40$ nm where the actual measured pin thickness is quite variable, ranging from <1 to 16 nm as shown in Figs. 1(d) and 1(e). This large pin thickness range contrasts strongly with the thinner, more uniform pins observed in optimized, conventionally processed Nb 47 wt % Ti, where the α-Ti ribbon thickness ranges from 1 to 5 nm.[1,3] Although there has been little explicit study of the role that the distribution in pin thickness plays, a wide distribution is almost certainly detrimental to J_c, as emphasized in recent studies of powder metallurgy APC composites.[11,30,31]

B. J_c vs d_p

The J_c vs d_p curves of Fig. 2 clearly illustrate that the optimum pin size is a function of magnetic field, the peak J_c moving towards smaller pin sizes as the field is increased. This agrees qualitatively with the results of Matsumoto *et al.*[9] with the exception that, at a given field, their pins optimized at approximately half the nominal pin diameter that is reported here. This difference may reflect the fact that their composite was made from a planar pin array, for which the ribbon structure may degrade less on extensive cold work than is the case for round pin arrays.

The difference in J_c behavior between the third and fourth extrusion composites of the present study must be related to a difference in their flux pinning microstructures. However, a comparison of the microstructures at $d_p=40$ nm, shown in Figs. 1(d) and 1(e), does not reveal any obvious differences between the average pin thickness or pin thickness distribution, for in both cases, the measured pin thickness varied from ~1 to 16 nm. A plausible explanation for the difference is that the fourth extrusion (carried out at 650 °C) caused additional pin/matrix interdiffusion. This could change the pinning microstructure in several ways, one way being that diffusion would tend to degrade the pin/matrix interface, thus diminishing the strength of the pinning wells. This appears to be the case at low fields where the J_c of the fourth extrusion composite is lower than that of the third. However, this is not the case at higher fields, where an enhancement of the fourth extrusion composite J_c is observed. Another consequence of interdiffusion which could explain this high field J_c enhancement is that the interdiffusion would serve to alloy the pins, thereby reducing their normal state coherence length, and causing the elementary pinning force to optimize for thinner pins.[20] Assuming, as usual, that full summation of the elementary pinning forces

occurs, this would lead to a relative enhancement of the high field J_c, as observed.

C. F_p curve shapes

Figures 1–4 present a clear picture of the microstructure and superconducting properties of this Nb pin APC composite as the pin size is reduced. The largest bulk pinning force occurred for pins whose measured average thickness was ~8 nm, a value which is considerably thicker than the 1–2 nm thick α-Ti ribbons found in optimized conventional Nb–Ti.[1,3] The greater optimum thickness of the Nb pin APC composite is in accordance with the magnetic pinning model,[20] which predicts that the pin thickness at which F_p is maximum is $\sim\xi_N/3$, where ξ_N is the pin proximity length. Measurements[32] show that the ξ_N of Ti is ~3 times shorter than that of Nb; the ξ_N of α-Ti is undoubtedly even shorter because it alloyed with ~5 at. % Nb.[1]

The magnetic pinning model[20] can also be used to describe the changes in $F_p(H)$ with decreasing pin size that occur in the present composite. At peak F_p (d_p=40 nm), the elementary pinning force f_p is slightly less than its maximum value and the pin thickness is approximately equal to $\xi_N/3$. Since $\xi_N/3$ is rather large for Nb pins (~27 nm),[32] the pin number density corresponding to pins of this thickness is low and this also corresponds to a fluxon density characteristic of low fields. As the pin size is reduced further, the pin density increases. However, the strong decrease in f_p which occurs for thinner pins cannot be properly compensated by the increase in pin-vortex interaction density. The net result is that $H_{\max}$ increases but the magnitude of $F_{p\,\max}$ decreases, as is clearly shown in Fig. 3.

D. H^*, H_{c2} measurements

That H_{c2} declines as d_p is reduced is clear from Fig. 4. As d_p is reduced from 165 to 15 nm, H_{c2}(4.2 K) declines from 10.3 to 9 T. This reduction is consistent with proximity-effect mixing of the matrix and pins at the final size. The overall composition of 76 vol % of Nb 47 wt % Ti matrix and 24 vol % Nb pins is Nb 32 wt % Ti, for which the homogeneous alloy mixture H_{c2} is ~9 T.[3] This agrees with the measured H_{c2} of 9 T in the APC wire at d_p=15 nm and is consistent with the conclusion that the pinning centers are fully coupled to the matrix.

Although H_{c2} is the critical field most often quoted for a superconductor, it is the irreversibility field H^* which is of real technological importance, because H^* defines the practical upper limit to J_c. Fortunately, in the case of optimized, conventional Nb 47 wt % Ti, the ~0.5 T (4.2 K) difference between H_{c2} and H^* is rather small. However, as shown in the inset graph of Fig. 4, in the APC wire for which F_p is maximum, i.e., d_p=40 nm, the quantity H_{c2}–H^* is ~0.9 T. This results in the optimized APC wire having an H^* value that is 1.6 T lower than in the optimized, conventional wire, clearly a severe obstacle to high field pinning.

Measurements of the irreversibility line $T_r(H)$ and $H_r(T)$ in conventional Nb–Ti wires[24] support the theory that the irreversibility line arises from a flux-lattice melting phase transition.[33] In high-temperature superconductors, it is found

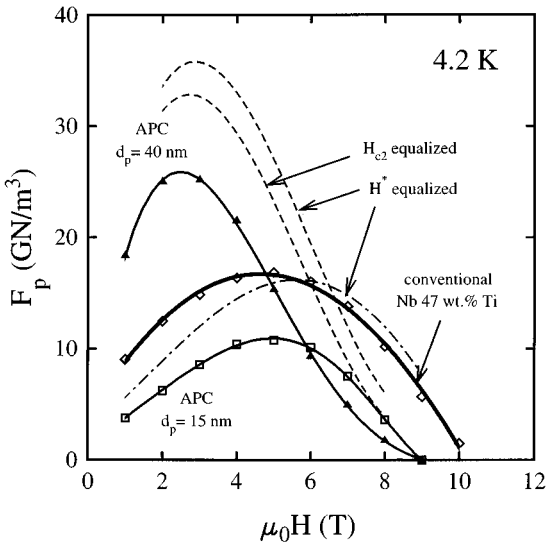

FIG. 5. F_p vs $\mu_0 H$ for d_p=40 and 15 nm at 4.2 K (solid lines) and at reduced temperatures (dashed lines) for which the H_{c2} and H^* values are approximately equal to the values for conventionally processed Nb 47 wt % Ti at 4.2 K. An optimized, conventional Nb 47 wt % Ti F_p curve (thick, solid line) is shown for comparison.

that H^* can be raised by adding stronger pinning centers. This does not appear to be the explanation here, since H_{c2}–H^* is maximum for d_p=40 nm, precisely the wire for which F_p is maximum. H^* reaches its minimum value at d_p=40 nm.

The value of H_{c2}–H^* may reflect the degree of proximity-effect mixing between the pins and the matrix. The inset graph of Fig. 4 shows how the quantity H_{c2}–H^* changes as the nominal pin diameter is reduced. At d_p=165 nm the pin shape is beginning to change, but the pin thickness is still fairly uniform and the difference between H_{c2} and H^* is only 0.4 T. By d_p=40 nm there is a fairly large distribution in pin thickness, as shown in Figs. 1(d) and 1(e). Thus, the degree of proximity-effect mixing may differ locally, producing a locally variable H_{c2}. By d_p=15 nm there may still be a wide distribution in Nb thickness (TEM at this pin size was inconclusive) but, for the most part, all the observable pins were thin enough (~1 nm) so that they should be completely proximity-effect coupled to the matrix. Such a two-phase nanostructure should be more electromagnetically homogeneous, thus reducing the difference between H^* and H_{c2}.

E. An effective comparison procedure for conventional and APC wires

Although the proximity-effect depression of H_{c2} in existing APC composite designs like the present severely limits the high field J_c, it is important to note that it does not pose any fundamental obstacle to developing high J_c in APC conductors. Figure 5 shows the F_p curves for the APC composite at d_p=40 nm (at which the highest F_p was achieved) and at d_p=15 nm (at which the highest F_p was achieved at >6 T), together with a curve for a high performance conventionally processed Nb–Ti wire.[26] Extrapolating the high field F_p of each curve to zero illustrates the pronounced differences

in their high field behavior. Table I shows that the measured H_{c2} of the conventional wire is between 1.2 and 1.6 T higher than the APC wires at d_p=40 and 15 nm. These differences were removed by lowering the measuring temperature of the APC wires, so that the H^* and H_{c2} values of the APC wires were equalized to 10.2 and 10.7 T. Table I shows that, at 3.5 K, the H_{c2} of the d_p=40 nm wire is 10.7 T, a value equal to that of the conventional wire at 4.2 K. Even by making this adjustment, H^* is still 0.6 T lower in the APC composite. By reducing the temperature even further to 3 K, the H^* values were equalized at 10.2 T. H^* was also equalized for d_p=15 nm by reducing the temperature to 3 K. The percentage increase in ΔM in going from 4.2 to 3.5 to 3 K was then applied to the 4.2 K transport F_p curves so as to construct the H_{c2} and H^* equalized F_p curves shown in Fig. 5. These equalized F_p curves clearly show that the Nb pin APC composite is superior to the conventional wire at all fields up to ~7 T. When H_{c2} was equalized, the APC composite achieved a J_c(5 T) of 4600 A/mm^2; when H^* was equalized, the J_c(5 T) increased to 5400 A/mm^2, a value which would be the highest J_c(5 T) ever reported in Nb–Ti, even higher than the 5200 A/mm^2 reported for a rolled conventional Nb–Ti tape[34] with aligned α-Ti ribbons oriented parallel to the applied field. Thus, it is quite clear that APC wires offer great promise for further raising the attainable J_c of Nb–Ti, particularly if the overall composition of matrix and pin can be better balanced so as to produce an overall Nb–Ti composition lying within the high H_{c2} range of Nb 42–48 wt % Ti.

The fact that the H_{c2} equalized APC composite performs only marginally better than the conventional wire at high fields further supports the assertion of Cooley *et al.*[20] that the pin proximity length is the defining parameter for determining the field at which $F_{p\,\max}$ will occur. As the authors suggested, a key to increasing the high field J_c of Nb–Ti may be in decreasing the pin proximity length.

V. CONCLUSIONS

The microstructure and superconducting properties J_c and H_{c2} have been thoroughly studied for an APC composite consisting of Nb 47 wt % Ti with 24 vol % of Nb pinning centers. A maximum bulk flux pinning force of 25 GN/m^3 occurred at $\sim 0.25 H_{c2}$ when the calculated nominal pin diameter was 40 nm. However, the actual pinning center thickness at this size ranged from <1 to 16 nm. As the pin size was further reduced, the F_p peak position shifted to higher fields and the peak magnitude decreased.

By reducing the temperature at which the APC wires were measured, the values of H_{c2} and H^* were equalized to the values for optimized, conventional Nb 47 wt % Ti to compensate for the nonoptimal composition of the matrix and pin mixture. At fields up to 7 T, the APC composite clearly outperformed the conventional wire, achieving a J_c(5 T) of 4600 A/mm^2 when H_{c2} was equalized.

ACKNOWLEDGMENTS

We gratefully acknowledge W. Starch, A. Squitieri, J. Marquardt, M. Pelletier, and Y. Chen for their technical assistance and A. Gurevich and L. Cooley for their helpful discussions. The work was supported by the Department of Energy–Division of High Energy Physics. The scanning electron microscopy was partially supported by the Integrated Microscopy Resource which is supported through NIH Biomedical Research Technology Grant RR 00570.

[1] P. J. Lee and D. C. Larbalestier, Acta. Metall. **35**, 2526 (1987).
[2] C. Li and D. C. Larbalestier, Cryogenics **27**, 171 (1987).
[3] C. Meingast, P. J. Lee, and D. C. Larbalestier, J. Appl. Phys. **66**, 5962 (1989).
[4] C. Meingast and D. C. Larbalestier, J. Appl. Phys. **66**, 5971 (1989).
[5] P. J. Lee, J. C. McKinnell, and D. C. Larbalestier, Adv. Cryogenic Eng. **34**, 1001 (1988).
[6] G. L. Dorofejev, E. Yu Klimenko, and S. V. Frolov, *Proceedings of the 9th International Conference on Magnet Technology*, edited by C. Marinucci and P. Weymuth (Swiss Institute for Nuclear Research, Villigen, Switzerland, 1985), p. 564.
[7] L. R. Motowidlo, B. A. Zeitlin, M. S. Walker, and P. Haldar, Appl. Phys. Lett. **61**, 991 (1992).
[8] J. Wong, US Patent, No. 5,230,748 (27 July 1993); J. Wong and M. K. Rudziak, US Patent Nos. 516,550 (3 Nov 1992) and 5,223,348 (29 June 1993); J. Wong, M. K. Rudziak, and D. W. Capone II, US Patent Nos. 5,158,620 (27 Oct. 1992) and 5,160,794 (3 Nov. 1992).
[9] K. Matsumoto, H. Takewaki, Y. Tanaka, O. Miura, K. Yamafuji, K. Funaki, M. Iwakuma, and T. Matsushita, Appl. Phys. Lett. **64**, 115 (1994).
[10] L. D. Cooley, P. J. Lee, D. C. Larbalestier, and P. M. O'Larey, Appl. Phys. Lett. **64**, 1928 (1994).
[11] P. D. Jablonski, P. J. Lee, and D. C. Larbalestier, Appl. Phys. Lett. **65**, 767 (1994).
[12] R. W. Heussner, P. D. Jablonski, P. J. Lee, and D. C. Larbalestier, IEEE Trans. Appl. Supercond. **5**, 1705 (1995).
[13] N. D. Rizzo, S. Ling, J. McCambridge, D. Prober, L. Motowidlo, and B. Zeitlin, Low Temperature Superconductor Workshop, Devil's Head, WI, 1994.
[14] P. G. deGennes, Rev. Mod. Phys. **36**, 225 (1964).
[15] K. Matsumoto, Y. Tanaka, K. Yamafuji, K. Funaki, M. Iwakuma, and T. Matsushita, IEEE Trans. Appl. Supercond. **3**, 1362 (1993).
[16] L. D. Cooley, Ph.D. thesis, University of Wisconsin-Madison, 1993.
[17] J. D. McCambridge, N. D. Rizzo, X. S. Ling, J. Q. Wang, and D. E. Prober, IEEE Trans. Appl. Supercond. **5**, 1697 (1995).
[18] E. Kadyrov, A. Gurevich, and D. C. Larbalestier, Appl. Phys. Lett. **68**, 1567 (1996).
[19] L. D. Cooley, P. J. Lee, and D. C. Larbalestier, IEEE Trans. Magn. **27**, 1096 (1991).
[20] L. D. Cooley, P. J. Lee, and D. C. Larbalestier, Phys. Rev. B **53**, 6638 (1996).
[21] L. D. Cooley, Adv. Cryo. Eng. (to be published).
[22] C. B. Nunes, R. W. Heussner, and D. C. Larbalestier, J. Appl. Phys. **80**, 1647 (1996).
[23] C. P. Bean, Rev. Mod. Phys. **36**, 31 (1964).
[24] M. Suenaga, A. K. Ghosh, Y. Xu, and D. O. Welch, Phys. Rev. Lett. **66**, 1777 (1991).
[25] L. A. Bonney, T. C. Willis, and D. C. Larbalestier, J. Appl. Phys. **77**, 6377 (1995).
[26] These data come from a 61 filament multifilamentary Nb 47 wt % Ti composite that was fabricated at UW-Madison and was designated CB9738. The composite processing included 3×80 h/420 °C heat treatments. It is one of the highest J_c multifilamentary Nb–Ti composites ever produced.
[27] J. F. Peck and D. A. Thomas, Trans. Met. Soc. AIME **221**, 1240 (1961).
[28] W. F. Hosford, Trans. Met. Soc. AIME **230**, 12 (1964).
[29] J. C. Malzahn Kampe and T. H. Courtney, Scripta Metall. **23**, 141 (1989).
[30] P. D. Jablonski, Ph.D. thesis, University of Wisconsin-Madison, 1994.
[31] P. J. Lee, P. D. Jablonski, and D. C. Larbalestier, IEEE Trans. Appl. Supercond. **5**, 1701 (1995).
[32] C. B. Nunes (unpublished).
[33] A. Houghton, R. A. Pelcovits, and S. Sudbo, Phys. Rev. B **40**, 6763 (1993).
[34] L. D. Cooley, P. D. Jablonski, P. J. Lee, and D. C. Larbalestier, Appl. Phys. Lett. **58**, 2984 (1991).